LVRT Strategy Considering Reactive Power Support and Fluctuating Power Suppression for Photovoltaic Application

Zhichao ZHANG, Qihang LIU, Yupei WANG

School of Electrical Engineering, China University of Mining and Technology, Xuzhou, 221008, China

zhichao_zhang123@163.com

Submitted April 12, 2025 / Accepted July 3, 2025 / Online first July 21, 2025

Abstract. *Addressing the insufficient negative sequence dynamic reactive current support and power doubling oscillations present in conventional low-voltage ride through control mechanisms for photovoltaic inverters, this study designs a q-axis command for both positive and negative sequence currents in accordance with recent regulatory requirements for photovoltaic grid integration technologies. The d-axis commands for positive and negative sequence currents are computed to effectively attenuate second harmonic fluctuations in active power output. The proposed approach establishes equilibrium between inverter current carrying capacity and oscillation mitigation, thereby concurrently enhancing dynamic reactive current support for both sequence components while diminishing power doubling fluctuations. The short-circuit current characteristics of photovoltaic installations are examined utilizing this enhanced low-voltage ride through control methodology. Comparative analysis between the suggested approach and current low-voltage ride through control techniques was conducted via simulation models, confirming both the efficiency of the proposed method and the accuracy of analytical expressions for short-circuit current.*

Keywords

Photovoltaic, low voltage ride through (LVRT), reactive power support, fluctuating power suppression, efficiency

1. Introduction

With the large-scale development of renewable energy, photovoltaic electricity generation capacity has experienced rapid expansion. IEEE and IEC regulations explicitly require photovoltaic installations to maintain low voltage ride through functionality during grid disturbances, thereby averting disconnection at connection points when grid voltage precipitously drops and preventing subsequent disruptions to network operational stability [1], [2].

The existing research explores two main ways to achieve low voltage ride through capability: one is by introducing specific hardware devices, and the other is by adjusting the control strategy of the inverter [3].

Regarding hardware implementation approaches, the active power absorption during grid anomalies via supplementary super energy storage units integrated into the photovoltaic dc circuit is demonstrated, which mitigates voltage elevation and enhances dc bus voltage stability [4]. Additionally, a static synchronous compensator (STATCOM) that supplies reactive power during voltage sags is employed in [5], thereby elevating and sustaining grid voltage levels and securing continuous connection of photovoltaic generation systems despite low voltage conditions. Although it is relatively easy to achieve dc bus voltage control by adding hardware equipment, the investment cost of hardware equipment is generally high, which is not conducive to economic cost control [6], [7].

Regarding control methodology modifications, the dual-phase photovoltaic grid-connected low-voltage ride through approach utilizing active power command allocation is introduced in [8], [9]. This methodology dynamically modifies grid-connected inverter active power commands according to grid voltage depression severity, communicating these adjustments to the dc-dc boost circuitry, enabling photovoltaic arrays to adaptively regulate output generation while preserving dc bus voltage stability [10]. The current carrying capacity of photovoltaic inverters, taking into account the dynamic reactive current support capability specified by photovoltaic grid connection technology is discussed in [11], [12], and a limiting strategy is proposed for active current. Nevertheless, this approach potentially induces dc voltage elevation during voltage sag conditions, possibly activating overvoltage protective mechanisms and resulting in photovoltaic system disconnection from the network. A model predictive current control-based low-voltage ride through technique that enhances grid voltage through inverter reactive current generation is proposed in [13–15]. Nonetheless, this methodology neglects dc voltage implications.

DOI: 10.13164/re.2025.0471

A low voltage ride through (LVRT) mechanism that reallocates current commands is introduced in [16] while maintaining constant power as the primary control target. This approach simultaneously satisfies current limitations while accomplishing multiple objectives: negative sequence current attenuation, mitigation of second harmonic oscillations in both active power and dc bus voltage, and reduction of reactive power second harmonic components [17]. However, the paper did not consider the dynamic reactive current support capability required by photovoltaic grid connection technology regulations. This standard explicitly requires that in the event of a symmetrical fault on the grid side, the photovoltaic power station should have the ability to support positive sequence dynamic reactive current [18]. Under asymmetrical grid disturbances, photovoltaic facilities must demonstrate dual capabilities: supporting both positive sequence and negative sequence dynamic reactive current.

Throughout fault intervals, photovoltaic grid-connected inverter control methodologies bifurcate into two distinct phases: constant power regulation and current limitation control [19–21]. Varying voltage depression magnitudes necessitate different control objectives for photovoltaic grid-connected inverters, consequently altering applicable current analytical expressions. During minor disturbances characterized by modest voltage reductions at grid interconnection points, voltage outer loop control circuitry maintains operational functionality. This mechanism encompasses accurate monitoring of dc bus voltage variations, with subsequent corrective actions implemented via proportional integral (PI) controllers to preserve dc bus voltage equilibrium [22], [23].

An analytical formula for calculating short-circuit current in photovoltaic power generation is proposed in [24], taking into account fluctuations in dc bus voltage. During constant power regulation phases in photovoltaic systems, this approach employs power conservation principles between dc and ac domains while accounting for dc voltage variations [25]. Through resolution of current's second-order differential equations, the methodology determines current command value oscillations [26]. However, this technique exclusively addresses dc components and voltage outer loop parameter effects while disregarding current inner loop dynamics and filtering element influences. During severe grid disturbances, inverters transition to current limitation mode, voltage outer loop functionality ceases, resulting in compromised dc bus voltage regulation [27].

The instantaneous power principles to examine power-voltage/current correlations is discussed in [28], deriving photovoltaic inverter short-circuit current expressions through fixed power objective establishment. This approach neglects regulatory specifications for dynamic reactive power support capabilities required from photovoltaic installations during fault conditions as stipulated in grid interconnection standards. The photovoltaic system steady-state currents is examined in [29], developing appropriate short-circuit current formulations for steady-state fault behavior characterization. However, this work omits analysis of transient fault phenomena. Therefore, the research results cannot be directly applied to analyze and calculate the transient characteristics of photovoltaic power generation system faults [30].

Addressing aforementioned challenges, this study presents a low voltage ride through control methodology that establishes equilibrium between dynamic reactive current support provision and active power second harmonic oscillation attenuation. This approach incorporates dynamic reactive current support requirements mandated by grid interconnection protocols while comprehensively addressing inverter current limitations, thereby optimizing power doubling oscillation mitigation during asymmetrical fault scenarios. Secondly, the steady-state and transient current analytical expressions of short-circuit current in photovoltaic electric fields under asymmetric fault conditions were analyzed. Using PSCAD/EMTDC simulation environment, a comprehensive photovoltaic grid-connected generation model was developed to validate both the efficacy of the presented low-voltage ride through methodology and the accuracy of derived short-circuit current mathematical expressions.

2. Photovoltaic System Mathematical Framework

Figure 1 illustrates the structural configuration of grid-connected photovoltaic generation system. Photovoltaic panels depicted generate low-level dc power, which undergoes voltage amplification via boost circuitry (BC) before conversion to ac power through voltage source converter (VSC), ultimately interfacing with utility networks via transmission line. Maximum power point tracking algorithms implemented within boost converters dynamically adjust photovoltaic panel output voltage, thereby ensuring optimal operational efficiency at peak power generation points.

The voltage source converter adopts a dual loop control architecture, which combines the design of voltage outer loop and current inner loop to achieve efficient decoupling control of voltage, greatly enhancing the flexibility and accuracy of system regulation.

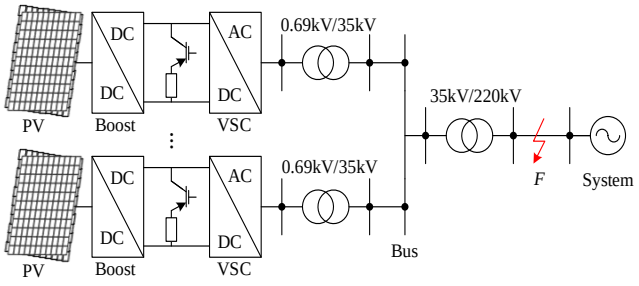

Fig. 1. Photovoltaic power generation grid-integration architecture.

When an asymmetric fault occurs at point F in the diagram, the instantaneous power delivered by the photovoltaic power station to the grid can be expressed as:

$$\begin{cases} P = P_0 + P_{S2}\sin(2\omega t) + P_{C2}\cos(2\omega t) \\ Q = Q_0 + Q_{S2}\sin(2\omega t) + Q_{C2}\cos(2\omega t) \end{cases} \tag{1}$$

where P and Q are the instantaneous power output of the inverter; P_0 and Q_0 are the instantaneous dc components of the inverter output power; P_{S2} and Q_{S2} are the sine power components output by the inverter; P_{C2} and Q_{C2} are the cosine power components output by the inverter.

Application of Park transformation to grid-side voltage and current yields component representations within synchronous rotating reference frames, facilitating power component characterization during fault conditions.

$$\begin{bmatrix} P_0 \\ P_{S2} \\ P_{C2} \\ Q_0 \\ Q_{S2} \\ Q_{C2} \end{bmatrix} = \begin{bmatrix} e_{dP} & e_{qP} & e_{dN} & e_{qN} \\ e_{qN} & -e_{dN} & -e_{qP} & e_{dP} \\ e_{dN} & e_{qN} & e_{dP} & e_{qP} \\ e_{qP} & -e_{dP} & e_{qN} & -e_{dN} \\ -e_{dN} & -e_{qN} & e_{dP} & e_{qP} \\ e_{qN} & -e_{dN} & e_{qP} & -e_{dP} \end{bmatrix} \begin{bmatrix} i_{dP} \\ i_{qP} \\ i_{dN} \\ i_{qN} \end{bmatrix} \tag{2}$$

where P and N represent positive and negative order; e_d and e_q are the d-axis and q-axis components of the grid voltage, respectively; i_d and i_q represent the d-axis and q-axis components of the grid current, respectively.

Equation (2) demonstrates that during asymmetrical grid faults, grid-connected inverters inherently lack sufficient control capability to regulate all six power components using only four independent current variables. Therefore, four independent current variables are usually used to control the four power components, which respectively satisfy three control strategies of suppressing negative sequence current, suppressing reactive second harmonic fluctuations, and suppressing active second harmonic fluctuations,

$$\begin{bmatrix} i_{dP}^* \\ i_{qP}^* \\ i_{dN}^* \\ i_{qN}^* \end{bmatrix} = \frac{2}{3}\begin{bmatrix} e_{dP} & e_{qP} \\ e_{qP} & -e_{dP} \\ -ke_{dN} & ke_{qN} \\ -ke_{qN} & -ke_{dN} \end{bmatrix}\begin{bmatrix} \dfrac{P_0^*}{M_1} \\ \dfrac{Q_0^*}{M_2} \end{bmatrix}, \tag{3}$$

$$\begin{cases} M_1 = (e_{dP})^2 + (e_{qP})^2 - k(e_{dN})^2 - k(e_{qN})^2 \\ M_2 = (e_{dP})^2 + (e_{qP})^2 + k(e_{dN})^2 + k(e_{qN})^2 \end{cases}$$

where i_d^* and i_q^* are the current command values; P_0^* and Q_0^* are the expected output power values of the inverter; k is the instruction for switching the inverter gear. When k is 1, it means suppressing the second harmonic fluctuation of active power. When k is −1, it means suppressing the second harmonic fluctuation of reactive power. When k is 0, it indicates the suppression of negative sequence current.

Appropriate inverter low voltage ride through control methodologies can be implemented through parametric adjustment of coefficient k.

Throughout low voltage ride through operations, current reference values fluctuate according to implemented control approaches, subsequently producing significantly divergent fault response characteristics in inverter output currents. From (3), it can be concluded that under a certain control strategy, by adjusting the values of two current commands, the values of the other two current commands can be derived accordingly. This relationship establishes the theoretical basis for forthcoming analysis of advanced low-voltage ride through control methodologies that simultaneously incorporate dynamic reactive current support while attenuating power oscillations.

3. Low Voltage Ride Through Control Methodology

3.1 LVRT Strategy Considering Reactive Current Support

Upon grid disturbance occurrence, photovoltaic grid interconnection technical standards explicitly mandate voltage ride through capabilities for photovoltaic installations during symmetrical faults, preventing system disconnection resulting from significant voltage depression while mitigating potential fault propagation. That is, in the event of a power grid failure, photovoltaic power plants need to have dynamic reactive current support capability, which can be expressed as:

$$\Delta I_t = K_1(0.9 - U_t)I_N, 0 \le U_t \le 0.9 \tag{4}$$

where ΔI_t is the dynamic reactive current increment injected into the photovoltaic power station; K_1 is the dynamic reactive current coefficient, with values ranging from 1.3 to 1.5; U_t is the voltage per unit value at the grid connection point; I_N is the rated current of the photovoltaic power station.

During asymmetrical fault conditions, photovoltaic systems must inject positive sequence reactive current comprising both nominal operational values and additional positive sequence reactive current increments. Concurrently, these installations must absorb negative sequence reactive current determined by differential values of negative sequence reactive current increments. The dynamic positive and negative sequence reactive current should respond to changes in voltage according to (5):

$$\begin{cases} \Delta I_{tP} = K_{2P}(0.9 - U_{tP})I_N \\ \Delta I_{tN} = K_{2N}U_{tN}I_N \end{cases} \tag{5}$$

where ΔI_{tP} and ΔI_{tN} are the positive sequence dynamic reactive current increment injected into the power grid and the negative sequence reactive current increment absorbed

from the power grid; K_{2P} and K_{2N} are proportional coefficients of positive and negative sequence currents, and their values should not be less than 1; U_{tP} and U_{tN} are the unit values of the positive and negative sequence components of the grid voltage; I_N is the rated current of the photovoltaic power station.

Equation (5) demonstrates that minor voltage depressions at grid interface points necessitate proportionally small reactive current contributions from photovoltaic installations, resulting in minimal inverter operational effects. Consequently, grid-side power oscillations remain negligible, eliminating requirements for power fluctuation mitigation techniques. At this point, the photovoltaic power station aims to provide only reactive power support, and the current command value i_{qP}^* and i_{qN}^* can be obtained for the grid connected inverter of the photovoltaic power station after an asymmetric fault occurs on the grid side,

$$\begin{cases} i_{qP}^* = i_{q0}^* + \Delta I_{tP} \\ i_{qN}^* = -\Delta I_{tN} \end{cases}. \tag{6}$$

During asymmetrical fault scenarios, positive sequence *d*-axis short-circuit current components require limitation according to (7), accounting for current capacity constraints in photovoltaic system grid-connected inverters:

$$i_{d\,Plim}^* = \sqrt{I_{MAXP}{}^2 - i_{qP}^{*2}} \tag{7}$$

where $i_{d\,Plim}^*$ is the amplitude limit of the *d*-axis positive sequence current command value; I_{MAXP} is the maximum value of positive sequence current.

Upon asymmetrical grid fault occurrence, inverter current references undergo recalculation through (6) and (7), facilitating photovoltaic system inverter compliance with dynamic positive and negative sequence reactive current support requirements during fault conditions. This is referred to as the LVRT1 strategy. The command current of the inverter under this low voltage ride through measure is:

$$\begin{cases} i_{dP}^* = i_{d\,Plim}^* \\ i_{qP}^* = i_{q0}^* + \Delta I_{tP} \\ i_{dN}^* = 0 \\ i_{qN}^* = -\Delta I_{tN} \end{cases}. \tag{8}$$

3.2 LVRT Strategy Considering Reactive Current Support and Power Fluctuation Suppression

During significant asymmetrical grid disturbances, inverter-delivered active power experiences amplified oscillatory behavior. Under these conditions, advanced LVRT control methodologies can simultaneously facilitate dynamic reactive current provision while attenuating power double-frequency oscillations.

Taking k as 1 to suppress the second harmonic fluctuation of active power, the command values for active and reactive power can be obtained,

$$\begin{cases} P_1^* = \dfrac{3M_1N_1}{2D} \\ Q_1^* = -\dfrac{3M_2N_2}{2D} \end{cases} \tag{9}$$

where $N_1 = e_{dN}\, i^*_{qP} - e_{dP}\, i^*_{qN}$, $N_2 = e_{qN}\, i^*_{qP} + e_{qP}\, i^*_{qN}$, $D = e_{qN}\, e_{qP} + e_{dP}\, e_{qN}$.

Incorporating dynamic reactive current support requirements during asymmetrical fault conditions with power reference formulations, the comprehensive active power, reactive power, and current reference parameters can be obtained as,

$$\begin{cases} i_{dP1}^* = \dfrac{e_{dP}N_1}{D} - \dfrac{e_{qP}N_2}{D} \\ i_{dN1}^* = -\dfrac{e_{dN}N_1}{D} - \dfrac{e_{qN}N_2}{D} \end{cases}. \tag{10}$$

Current reference reconfiguration satisfies dynamic reactive current support criteria while effectively attenuating active power second harmonic oscillations. At this time, the current command value of the inverter is,

$$\begin{cases} i_{dP}^* = i_{dP1}^* \\ i_{qP}^* = i_{q0}^* + \Delta I_{tP} \\ i_{dN}^* = i_{dN1}^* \\ i_{qN}^* = -\Delta I_{tN} \end{cases}. \tag{11}$$

As the severity of power grid faults increases, the dynamic reactive current support required by photovoltaic power stations will correspondingly increase. Considering that the current command value calculated through (9)–(11) may exceed the limit, it is necessary to perform amplitude limiting on the current command value. Positive and negative sequence *q*-axis current references require configuration in accordance with photovoltaic grid interconnection technical standards to facilitate dynamic reactive current support while maintaining grid connectivity. This paper limits the current command value i_{aP}^*. When the current command value i_{aP}^* decreases and does not meet the limit requirements, then limit the current command value i_{aN}^*.

Positive and negative sequence currents maintain phase relationships as illustrated in Fig. 2. In Fig. 2, I^+ is the positive sequence current, I^- is the negative sequence current, I_{MAX} is the maximum current flowing through the inverter, and $\Delta\varphi$ is the absolute value of the phase difference between the positive and negative sequence currents.

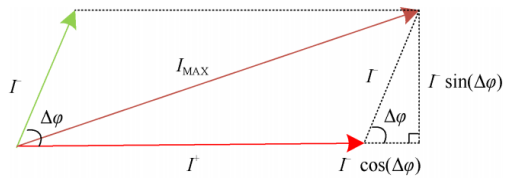

Fig. 2. Phase vector relationship between positive and negative sequence current.

The absolute phase differential between positive and negative sequence current vectors can be mathematically formulated as:

$$\Delta\varphi = \left|\arctan\frac{i_{\mathrm{qP}}}{i_{\mathrm{dP}}} - \arctan\frac{i_{\mathrm{qN}}}{i_{\mathrm{dN}}}\right|. \tag{12}$$

Geometric analysis of Fig. 2 enables determination of relational constraints between positive and negative sequence current vectors relative to maximum permissible inverter current magnitude. Utilizing these vectorial relationships, maximum positive sequence current magnitude I_{MAXP} can be derived:

$$I_{\mathrm{MAXP}} = \sqrt{I_{\mathrm{MAX}}^2 - \left(I^- \sin(\Delta\varphi)\right)^2} - I^- \cos(\Delta\varphi)\,. \tag{13}$$

Considering the maximum current carrying capacity of the inverter, calculate the amplitude limit of i_{aP}^*:

$$i_{\mathrm{dPlim}}^* = \sqrt{I_{\mathrm{MAXP}}^2 - i_{\mathrm{qP}}^{*2}}. \tag{14}$$

Based on the above analysis, when an asymmetric fault occurs on the grid side, taking into account the low voltage ride through strategy (referred as LVRT2 strategy) that supports dynamic reactive current and suppresses the second harmonic fluctuation of active power, the current command value is shown in (15) when the inverter limits i_{dP}^*.

$$\begin{cases} i_{\mathrm{dP}}^* = \min\left(i_{\mathrm{dP1}}^*, i_{\mathrm{dPlim}}^*\right) \\ i_{\mathrm{qP}}^* = i_{\mathrm{qP0}}^* + \Delta I_{\mathrm{tP}} \\ i_{\mathrm{dN}}^* = i_{\mathrm{dN1}}^* \\ i_{\mathrm{qN}}^* = -\Delta I_{\mathrm{tN}} \end{cases}. \tag{15}$$

Following acquisition of voltage and current positive and negative sequence components within dq reference frames, appropriate LVRT control methodologies can be implemented according to grid connection point voltage depression severity. This investigation establishes a 0.8 p.u. voltage threshold at grid interface points as the demarcation criterion between minor and significant grid-side disturbances; based on this, switch between the "LVRT strategy that only provides reactive current support" and the "LVRT strategy that takes into account dynamic reactive current support and suppresses power doubling frequency fluctuations". Positive and negative sequence current references are computed through (8) and (15). These sequence-specific current references subsequently feed into respective positive and negative sequence current control loops, facilitating precise current trajectory regulation. After

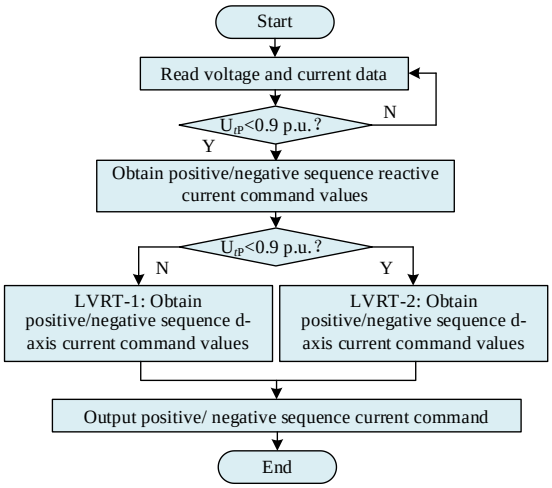

Fig. 3. Flowchart of low voltage ride through control.

Condition	i_{dP}^*	i_{qP}^*	I_{dN}^*	i_{qN}^*
Normal	a_0	b_0	c_0	d_0
Minor fault	a_1	b_1	c_1	d_1
Severe fault	a_2	b_2	c_2	d_2

Tab.1. Switching table of current instruction values.

a rapid transient process, the inverter outputs a steady-state value that is almost equal in magnitude to the command value, thereby accomplishing LVRT performance objectives. Figure 3 illustrates the LVRT control process implementation during grid fault conditions.

Table 1 presents inverter current reference transition scenarios during asymmetrical grid disturbances, derived from the reference calculation methodologies.

Figure 4 depicts the comprehensive LVRT control system architecture. From the developed LVRT control frameworks, photovoltaic system grid-connected inverters implement differential control responses during asymmetrical grid faults according to connection point voltage depression magnitudes, maintaining compliance with grid interconnection technical standards. During voltage depressions exceeding 0.2 p.u., implemented LVRT methodologies simultaneously satisfy dynamic reactive power support requirements while attenuating active power second

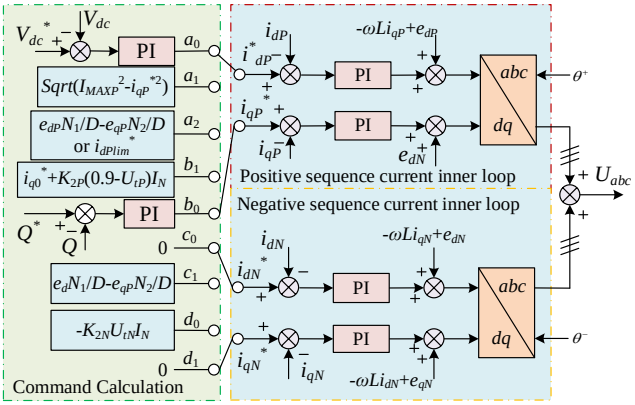

Fig. 4. LVRT strategy for suppressing double frequency active power fluctuation based on reactive current support.

harmonic components in transmitted power. In asymmetric faults, photovoltaic power plants need to absorb negative sequence reactive power from the grid, necessitating non-zero negative sequence current components. This requisite negative sequence current presence during asymmetrical disturbances fundamentally contradicts LVRT strategies predicated upon negative sequence current suppression. Consequently, the LVRT methodologies proposed herein are incompatible with negative sequence current suppression approaches. By switching the instantaneous current command value of the fault, the changes in the command value can be obtained, establishing the theoretical foundation for subsequent short-circuit current quantification analyses.

4. Short Circuit Current in LVRT Strategy

Figure 5 shows the operating principle of the inverse type grid connected converter. In Fig. 5, e_a, e_b, and e_c are the grid voltage, i_a, i_b, and i_c are the grid current, L is the AC filter inductor, R is the AC filter resistor, i_{dc} and u_{dc} are the DC bus current and DC bus voltage, and S1–S6 are IGBT switches.

When operating under unbalanced conditions, negative sequence voltage components emerge within the system. For grid-tied inverters, the voltage components of both positive and negative sequences expressed in the synchronously rotating dq reference frame are:

$$\begin{cases} V_{\mathrm{dP}} = e_{\mathrm{dP}} + L\dfrac{\mathrm{d}i_{\mathrm{dP}}}{\mathrm{d}t} + Ri_{\mathrm{dP}} - \mathrm{j}\omega Li_{\mathrm{qP}} \\ V_{\mathrm{qP}} = e_{\mathrm{qP}} + L\dfrac{\mathrm{d}i_{\mathrm{qP}}}{\mathrm{d}t} + Ri_{\mathrm{qP}} + \mathrm{j}\omega Li_{\mathrm{dP}} \\ V_{\mathrm{dN}} = e_{\mathrm{dN}} + L\dfrac{\mathrm{d}i_{\mathrm{dN}}}{\mathrm{d}t} + Ri_{\mathrm{dN}} + \mathrm{j}\omega Li_{\mathrm{qN}} \\ V_{\mathrm{qN}} = e_{\mathrm{qN}} + L\dfrac{\mathrm{d}i_{\mathrm{qN}}}{\mathrm{d}t} + Ri_{\mathrm{qN}} - \mathrm{j}\omega Li_{\mathrm{dN}} \end{cases} \tag{16}$$

where V_{dP} and V_{qP} are the output voltages in the positive sequence dq coordinate system; V_{dN} and V_{qN} are the output voltages in the negative sequence dq coordinate system; e_{dP} and e_{qP} represent the grid voltage in the positive sequence dq coordinate system; e_{dN} and e_{qN} are the voltage vectors of the power grid in the negative sequence dq coordinate system; L, R is the equivalent filtering inductance and resistance of the inverter; ω is the angular frequency of the grid voltage; i_{dP} and i_{qP} are the output currents in the positive sequence dq coordinate system; i_{dN} and i_{qN} are the output currents in the negative sequence dq coordinate system. K_{PP}, K_{IP} are the proportional and integral control parameters, respectively, for the positive-sequence current inner-loop. They are used in the proportional-integral (PI) controller for positive-sequence current control. K_{PN}, K_{IN} are the proportional and integral control parameters, respectively, for the negative-sequence current inner-loop. They are used in the proportional-integral (PI) controller for negative-sequence current control. s is the complex variable in the Laplace domain. It is used in the transfer function representation of the PI controller. ω is the angular frequency of the grid voltage. j is the imaginary unit in the complex number system, where $\mathrm{j}^2 = -1$. L represents the inductance value in the electrical circuit. It is used to calculate the voltage drop across the inductor due to the current flow.

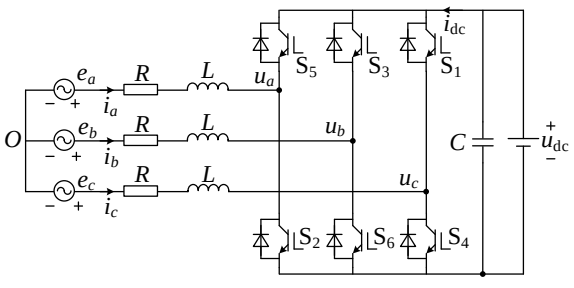

Fig. 5. Operating principle of grid-connected inverter.

Within typical circuit configurations, equivalent inductance L substantially exceeds the equivalent resistance R in magnitude, allowing for the omission of R in analytical considerations. Asymmetric fault conditions introduce negative sequence currents into the system, necessitating separate control mechanisms for both positive and negative sequence components. Equation (17) illustrates the control implementation for positive and negative sequence currents within the inner current control loop.

$$\begin{cases} V_{\mathrm{dP}} = e_{\mathrm{dP}} + \left(K_{\mathrm{PP}} + \dfrac{K_{\mathrm{IP}}}{s}\right)\left(i_{\mathrm{dP}}^{*} - i_{\mathrm{dP}}\right) - \mathrm{j}\omega Li_{\mathrm{qP}} \\ V_{\mathrm{qP}} = e_{\mathrm{qP}} + \left(K_{\mathrm{PP}} + \dfrac{K_{\mathrm{IP}}}{s}\right)\left(i_{\mathrm{qP}}^{*} - i_{\mathrm{qP}}\right) + \mathrm{j}\omega Li_{\mathrm{dP}} \\ V_{\mathrm{dN}} = e_{\mathrm{dN}} + \left(K_{\mathrm{PN}} + \dfrac{K_{\mathrm{NN}}}{s}\right)\left(i_{\mathrm{dN}}^{*} - i_{\mathrm{dN}}\right) + \mathrm{j}\omega Li_{\mathrm{qN}} \\ V_{\mathrm{qN}} = e_{\mathrm{qN}} + \left(K_{\mathrm{PN}} + \dfrac{K_{\mathrm{IN}}}{s}\right)\left(i_{\mathrm{qN}}^{*} - i_{\mathrm{qN}}\right) - \mathrm{j}\omega Li_{\mathrm{dN}} \end{cases} \tag{17}$$

where K_{pp} and K_{Ip} are the PI control parameters of the positive sequence current inner loop; K_{pN} and K_{IN} are the PI control parameters for the negative sequence current inner loop; i_{dP}^{*} and i_{qP}^{*} are positive sequence current commands; i_{dN}^{*} and i_{qN}^{*} are negative sequence current commands.

By using (16) and (17), the second-order differential equation of the inverter output current can be derived:

$$\begin{cases} \dfrac{\mathrm{d}^2 i_{\mathrm{dP}}}{\mathrm{d}t^2} + \dfrac{K_{\mathrm{PP}}}{L}\dfrac{\mathrm{d}i_{\mathrm{dP}}}{\mathrm{d}t} + \dfrac{K_{\mathrm{IP}}}{L}i_{\mathrm{dP}} = \dfrac{K_{\mathrm{IP}}}{L}i_{\mathrm{dP}}^{*} \\ \dfrac{\mathrm{d}^2 i_{\mathrm{qP}}}{\mathrm{d}t^2} + \dfrac{K_{\mathrm{PP}}}{L}\dfrac{\mathrm{d}i_{\mathrm{qP}}}{\mathrm{d}t} + \dfrac{K_{\mathrm{IP}}}{L}i_{\mathrm{qP}} = \dfrac{K_{\mathrm{IP}}}{L}i_{\mathrm{qP}}^{*} \\ \dfrac{\mathrm{d}^2 i_{\mathrm{dN}}}{\mathrm{d}t^2} + \dfrac{K_{\mathrm{PN}}}{L}\dfrac{\mathrm{d}i_{\mathrm{dN}}}{\mathrm{d}t} + \dfrac{K_{\mathrm{IN}}}{L}i_{\mathrm{dN}} = \dfrac{K_{\mathrm{IN}}}{L}i_{\mathrm{dN}}^{*} \\ \dfrac{d^2 i_{\mathrm{qN}}}{\mathrm{d}t^2} + \dfrac{K_{\mathrm{PN}}}{L}\dfrac{\mathrm{d}i_{\mathrm{qN}}}{\mathrm{d}t} + \dfrac{K_{\mathrm{IN}}}{L}i_{\mathrm{qN}} = \dfrac{K_{\mathrm{IN}}}{L}i_{\mathrm{qN}}^{*} \end{cases} . \tag{18}$$

In (18), the set value of the current command is directly affected by the selection of the low voltage ride through control strategy. Different control strategies play a decisive role in setting the command values for positive and negative sequence currents. These differentiated instruction values will directly determine the current output characteristics under fault conditions.

Due to the continuity of current at the moment of fault occurrence, the definite solution conditions for the second-order differential equation of current can be obtained:

$$\begin{cases} i_{\mathrm{dP}} = i_{\mathrm{dP0}} \\ i_{\mathrm{qP}} = i_{\mathrm{qP0}} \end{cases} \tag{19}$$

where i_{dP0} is the positive sequence current of the *d*-axis before the fault; i_{qP0} is the positive sequence current of the *q*-axis before the fault.

Under standard operating conditions, negative sequence components are absent from the system, yielding the following definite solution for the negative sequence current second-order differential equation:

$$\begin{cases} i_{\mathrm{dN}} = 0 \\ i_{\mathrm{qN}} = 0 \end{cases}. \tag{20}$$

Applying the boundary conditions specified in (19) and (20) allows derivation of the analytical expression for the current second-order differential equation as:

$$\begin{cases} i_{\mathrm{dP}} = i_{\mathrm{dP}}^{*} + C_{1\mathrm{dP}}\,\mathrm{e}^{\lambda_{1\mathrm{dPt}}} + C_{2\mathrm{dP}}\,\mathrm{e}^{\lambda_{2\mathrm{dPt}}} \\ i_{\mathrm{qP}} = i_{\mathrm{qP}}^{*} + C_{1\mathrm{qP}}\,\mathrm{e}^{\lambda_{1\mathrm{qPt}}} + C_{2\mathrm{qP}}\,\mathrm{e}^{\lambda_{2\mathrm{qPt}}} \\ i_{\mathrm{dN}} = i_{\mathrm{dN}}^{*} + C_{1\mathrm{dN}}\,\mathrm{e}^{\lambda_{12\mathrm{Nt}}} + C_{2\mathrm{dN}}\,\mathrm{e}^{\lambda_{2\mathrm{dNt}}} \\ i_{\mathrm{qN}} = i_{\mathrm{qN}}^{*} + C_{1\mathrm{qN}}\,\mathrm{e}^{\lambda_{1\mathrm{qNt}}} + C_{2\mathrm{qN}}\,\mathrm{e}^{\lambda_{2\mathrm{qNt}}} \end{cases} \tag{21}$$

Through the resolution of second-order differential equations representing positive and negative sequence currents, one can derive theoretical analytical expressions for grid-connected positive and negative sequence currents within the *dq* reference frame. The equation transformation into a three-phase reference frame is achieved by applying the Parker inverse transformation method. The theoretical calculation formula for positive sequence three-phase current is:

$$\begin{cases} i_{\mathrm{a}} = \left(i_{\mathrm{dP}} + \mathrm{j}i_{\mathrm{qP}}\right)\mathrm{e}^{\mathrm{j}\omega t} + \left(i_{\mathrm{dN}} + \mathrm{j}i_{\mathrm{qN}}\right)\mathrm{e}^{-\mathrm{j}\omega t} \\ i_{\mathrm{b}} = \left(i_{\mathrm{dP}} + \mathrm{j}i_{\mathrm{qP}}\right)\mathrm{e}^{\mathrm{j}\omega t}\mathrm{e}^{-\mathrm{j}2\pi/3} + \left(i_{\mathrm{dN}} + \mathrm{j}i_{\mathrm{qN}}\right)\mathrm{e}^{-\mathrm{j}\omega t}\mathrm{e}^{-\mathrm{j}2\pi/3} \\ i_{\mathrm{c}} = \left(i_{\mathrm{dP}} + \mathrm{j}i_{\mathrm{qP}}\right)\mathrm{e}^{\mathrm{j}\omega t}\mathrm{e}^{\mathrm{j}2\pi/3} + \left(i_{\mathrm{dN}} + \mathrm{j}i_{\mathrm{qN}}\right)\mathrm{e}^{-\mathrm{j}\omega t}\mathrm{e}^{\mathrm{j}2\pi/3} \end{cases} \tag{22}$$

The output current in the *dq* coordinate system can be calculated through second-order differential equations. Use the Parker inverse transform to convert the short-circuit current in the *dq* coordinate system into the short-circuit current in the three-phase time-domain coordinate system. Three-phase short-circuit current comprises both initial transient components during fault inception and subsequent steady-state elements following fault stabilization.

To conclude, inverter output current fault characteristics during grid asymmetric disturbances are fundamentally determined by inner current loop control parameters and reference values established by various LVRT control approaches. Voltage sag magnitude at the point of grid interconnection serves as the critical determinant for LVRT strategy selection and implementation.

5. Case Analysis

5.1 Case Description

A simulation model based on the photovoltaic grid integration system depicted in Fig. 1 was constructed using PSCAD/EMTDC software environment. The system configuration includes a photovoltaic array with 30 MW rated capacity. Power generated from the photovoltaic installation flows via an inverter, undergoes voltage elevation through a 0.69 kV/35 kV box transformer before connection to the primary transformer (35 kV/220 kV). It is then sent out through an ac transmission line and integrated into the main power grid. The direct current bus operates at 1 kV voltage level. Current output has been constrained to a maximum of 1.2 per unit. The equivalent inductance of the filter is 0.825 mH. The fault occurred within 4 seconds. Within the positive sequence current internal control loop, proportional gain (K_{pp}) and integral gain (K_{Ip}) parameters were configured as 0.25 and 50, respectively. For the negative sequence current regulation loop, proportional (K_{pN}) and integral (K_{IN}) constants were established at 0.2 and 50, respectively.

5.2 Result Analysis

There is a phase-to-phase fault between point F and BC in Fig. 1. When experiencing fault conditions characterized by machine-end positive sequence voltage of 0.7 per unit alongside negative sequence voltage of 0.4 per unit, the photovoltaic station's grid-tied inverter implements techniques for negative sequence current suppression during low voltage ride through. Figure 6(a) presents simulation outcomes depicting power variation characteristics. It can be seen that the control strategy of suppressing negative sequence current will cause the active and reactive power delivered by the photovoltaic inverter to the grid side to fluctuate twice, and the amplitude of the fluctuation depends on the severity of the fault.

Figure 6(b) shows the three-phase current waveforms resulting from implementing negative sequence current suppression during low voltage ride through conditions. Analysis reveals that negative sequence current suppression methodology effectively regulates inverter short-circuit current output during grid asymmetric fault scenarios, maintaining approximate three-phase symmetry and delivering balanced currents to the grid network.

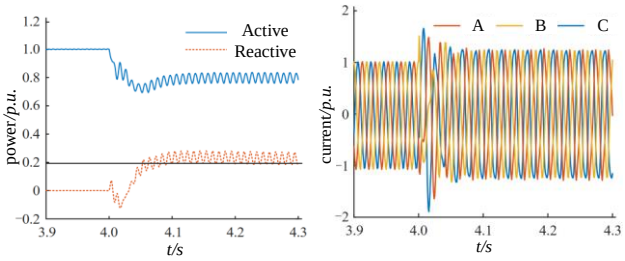

(a) Active and reactive power (b) Three phase current

Fig. 6. Power fluctuation and current during negative sequence current suppression LVRT operation.

Compliance with photovoltaic grid integration standards regarding negative sequence reactive current absorption necessitates modification of current reference values to enhance negative sequence reactive current uptake during grid asymmetric fault conditions. Figure 7(a) shows the simulation outcomes. These findings demonstrate that inverter reference value adjustments cause the photovoltaic facility to extract specific quantities of reactive current from the network, consequently lowering the reactive power equilibrium point. During this process, due to the constraints of the inverter's own current carrying capacity, the active power output will inevitably experience a certain degree of attenuation.

Figure 7(b) presents three-phase current simulation data when implementing LVRT with exclusive reactive current compensation. When employing negative sequence suppression techniques, *dq* axis negative sequence currents remain at zero, preventing negative sequence current emission from the photovoltaic installation. Conversely, when considering dynamic reactive current-assisted LVRT control methodology, the negative sequence *q*-axis current generates specific magnitudes, indicating that the photovoltaic system both consumes negative sequence current and contributes negative sequence dynamic reactive support. Due to the presence of negative sequence current, the balance of the three-phase current output by the inverter will be disrupted, resulting in a certain degree of asymmetry. However, merely modifying negative sequence *q*-axis current reference signals still introduces potential second harmonic oscillations in both active and reactive power delivery from the photovoltaic facility. Consequently, to maximize inverter active power stability, this research integrates active power second harmonic oscillation mitigation with sequence-based dynamic reactive current provision mandates from grid integration protocols, establishing an enhanced LVRT approach that simultaneously addresses power fluctuation concerns while fulfilling regulatory reactive support obligations.

Figure 8 presents comparative analysis of active and reactive power characteristics following implementation of active power second harmonic oscillation mitigation techniques. Figure 8(a) demonstrates that concurrent application of active power harmonic attenuation methods alongside reactive current compensation mechanisms substantially minimizes inverter active power oscillations. Figure 8(b) reveals that application of active power harmonic

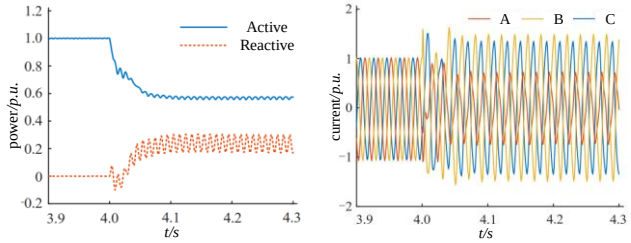

(a) Active and reactive power (b) Three phase current

Fig. 7. Power variation when only reactive current is provided to support low voltage ride through.

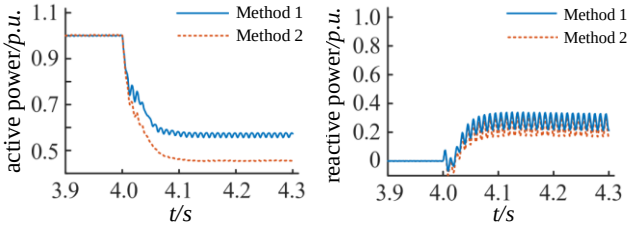

(a) Active power (b) Reactive power

Fig. 8. Comparison assessment of active and reactive power performance under alternative control methodologies.

damping protocols induces modifications in reactive power variation patterns, resulting in modest amplification of fluctuation magnitude.

Figure 9 illustrates positive and negative sequence *dq* axis current profiles with and without supplementary active power harmonic oscillation mitigation algorithms. Owing to regulatory mandates regarding dynamic reactive current provision in photovoltaic grid integration standards, *q*-axis positive and negative sequence currents depicted in Fig. 9, determined according to voltage sag severity, remain unaltered. From this, it can be seen that by changing the positive and negative sequence currents of the *d*-axis, the effect of suppressing the second harmonic fluctuation of active power has been achieved. This result is consistent with the previous analysis.

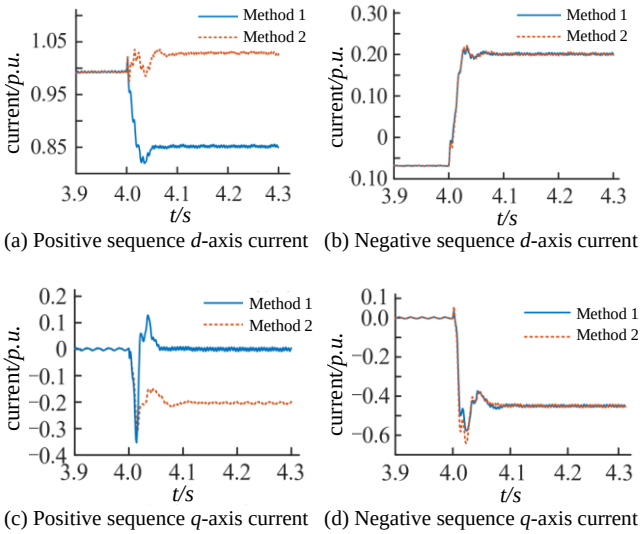

(a) Positive sequence *d*-axis current (b) Negative sequence *d*-axis current

(c) Positive sequence *q*-axis current (d) Negative sequence *q*-axis current

Fig. 9. Comparison of positive and negative sequence *dq* axis current between strategy 1 and strategy 2.

Simulation results demonstrate that our implemented LVRT control approach effectively mitigates active power second harmonic oscillations. This methodology satisfies all requirements for dynamic reactive current support across both sequence components as mandated by PV grid interconnection standards, while simultaneously achieving excellent active power harmonic oscillation reduction. However, applying this model toward reactive power harmonic oscillation mitigation yields simulation outcomes that potentially diverge from real-world behavior, indicating limitations in its applicability for reactive power harmonic control.

Figure 10 presents comparative results between theoretical calculations and simulation data for *dq* axis current components (both sequences) during a BC phase fault at location F (Fig. 1), characterized by sequence voltages of 0.7 p.u. (positive) and 0.4 p.u. (negative).

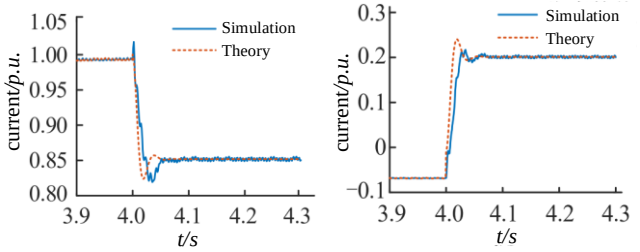

(a) Positive sequence *d*-axis current (b) Negative sequence *d*-axis current

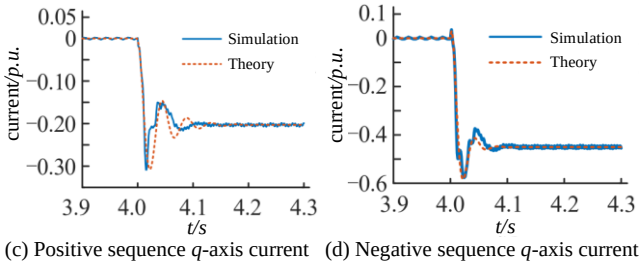

(c) Positive sequence *q*-axis current (d) Negative sequence *q*-axis current

Fig. 10. Theoretical and simulation comparison of *dq* axis current.

Figure 10 illustrates that during normal operation at unity power factor, the PV system exhibits control-influenced behavior with *d*-axis current oscillating near 1 p.u. and *q*-axis current varying around –0.06 p.u. Upon fault initiation, the control system dynamically adjusts its LVRT strategy according to voltage sag severity. This strategic adaptation triggers current reference reallocation. The variation of the current command value will trigger a series of dynamic changes in the current response, and this response process is closely related to the analytical formula of the second-order differential equation derived in detail in the previous text. Results depicted in Fig. 10 reveal abrupt transitions in *dq* axis current sequence components coinciding with fault inception, with exceptional correlation between simulation results and theoretical calculations.

Figure 11 displays comparative assessment between theoretical predictions and simulation results for three-phase current behavior. From Fig. 11, it can be seen that the

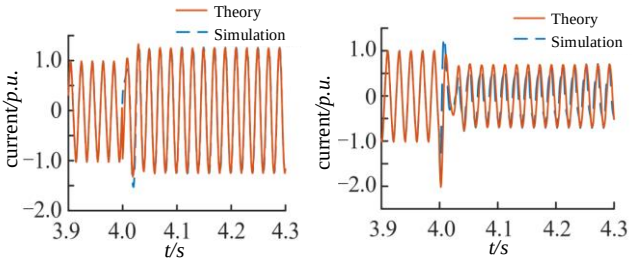

(a) Current of phase A (b) Current of phase B

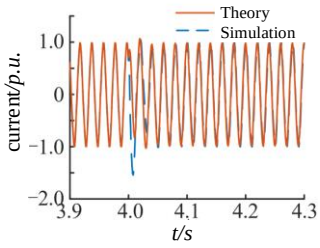

(c) Current of phase C

Fig. 11. Theoretical and simulation comparison of three-phase current.

three-phase currents calculated by (22) have a high degree of agreement with the simulated values.

Based on above experimental result, a comprehensive comparison is shown in Tab. 2, including droop control-based LVRT strategy [31], sliding-mode controller for power fluctuation suppression [32], traditional PI controller for LVRT [33]. It can be seen that the proposed method stands out with its adaptive reactive power range of 0.3–1.2 p.u. This adaptability enables it to respond more flexibly to varying grid conditions, potentially providing optimal reactive power compensation. In terms of fluctuation suppression, it limits rated-power fluctuation to ≤ 3%, which is superior to the other strategies. A lower fluctuation level helps maintain grid stability and reduces impacts on connected equipment. With a “moderate” complexity, it balances performance and implementation difficulty. Literature [31] uses a fixed reactive power of 0.8 p.u. While its complexity is “low”, the ~8% rated-power fluctuation is relatively high, which may cause greater grid disturbances. Literature [32] has a fixed 1.0 p.u. reactive power and high complexity, along with a ≤ 5% fluctuation. Though the fluctuation is better than [31], the high complexity may increase implementation costs. Literature [33] has an adaptive 0.5–1.0 p.u. reactive power and low complexity, but the ~10% fluctuation is the highest, making it less effective in suppressing power fluctuations. Overall, the proposed method shows a favorable trade-off among the key performance indicators.

Strategy	Reactive Power	Fluctuation Suppression	Complexity
Proposed Method	Adaptive (0.3–1.2 p.u.)	≤3% rated power	Moderate
[31]	Fixed (0.8 p.u.)	~8% rated power	Low
[32]	Fixed (1.0 p.u.)	≤5% rated power	High
[33]	Adaptive (0.5–1.0 p.u.)	~10% rated power	Low

Tab.2. Comprehensive comparison for different methods.

6. Conclusion

A novel low-voltage ride through (LVRT) approach is presented in this study, which simultaneously addresses positive and negative sequence reactive current support while mitigating active power second harmonic oscillations in grid-connected photovoltaic systems. Building upon this framework, an analysis of photovoltaic system short-circuit current behavior under asymmetric conditions yields several significant findings:

1) Conventional approaches focusing on negative sequence current suppression during grid asymmetric faults typically generate power doubling oscillations. Additionally, photovoltaic installations must absorb negative sequence reactive current—a requirement that contradicts the fundamental objectives of negative sequence current suppression in standard LVRT techniques.

2) Validation confirms the efficacy of our proposed LVRT methodology. During minor fault conditions, this approach satisfies all dynamic reactive current support requirements for both sequence components. In severe fault scenarios, our strategy not only fulfills dynamic reactive current support criteria across both sequence components but also effectively eliminates active power frequency doubling fluctuations.

3) An analytical expression for photovoltaic system short-circuit current is built for incorporating both sequence components of dynamic reactive current support and mechanisms for power doubling fluctuation mitigation. The theoretical results are highly consistent with the experimental results.

References

[1] XUE, Y., CHANG, L., KJAER, S. B., et al. Topologies of single-phase inverters for small distributed power generators: An overview. *IEEE Transactions on Power Electronics*, 2004, vol. 19, no. 5, p. 1305–1314. DOI: 10.1109/TPEL.2004.833460

[2] TEODORESCU, R., LISERRE, M., RODRIGUEZ, P. *Grid Converters for Photovoltaic and Wind Power Systems.* Hoboken (USA): Wiley, 2011. DOI:10.1002/9780470667057

[3] BLAABJERG, F., YANG, Y., YANG, D., et al. Distributed power generation systems and protection. *Proceedings of IEEE*, 2017. vol. 105, no. 7, p. 1311–1331. DOI: 10.1109/JPROC.2017.2696878

[4] TURITSYN, K., SULC, P., BACKHAUS, S., et al. Options for control of reactive power of distributed photovoltaic generators. *Proceedings of IEEE*, 2011. vol. 99, no. 6, p. 1063–1073. DOI: 10.1109/JPROC.2011.2116750

[5] DEMIROK, E., GONZÁLEZ, P. C., FREDERIKSEN, K. H. B., et al. Local reactive power control methods for overvoltage prevention of distributed solar inverters in low-voltage grids. *IEEE Journal of Photovoltaics*, 2011, vol. 1, no. 2, p. 174–182. DOI: 10.1109/JPHOTOV.2011.2174821

[6] CIOBOTARU, M., AGELIDIS, V. G., TEODORESCU, R., et al. Accurate and less-disturbing active anti-islanding method based on PLL for grid-connected converters. *IEEE Transactions on Power Electronics*, 2010, vol. 25, no. 6, p. 1576–1584. DOI: 10.1109/TPEL.2010.2040088

[7] ENSLIN, J. H. R., HESKES, P. J. M. Harmonic interaction between a large number of distributed power inverters and the distribution network. *IEEE Transactions on Power Electronics*, 2004, vol. 19, no. 6, p. 1586–1593. DOI: 10.1109/TPEL.2004.836615

[8] LI, X. ZHANG, H., SHADMAND, M. B., et al. Model predictive control of a voltage-source inverter with seamless transition between islanded and grid-connected operations. *IEEE Transactions on Industrial Electronics*, 2017, vol. 64, no. 10, p. 7906–7918. DOI: 10.1109/TIE.2017.2696459

[9] SAJADIAN, S., AHMADI, R. Model predictive control of dual-mode operations z-source inverter: Islanded and grid-connected. *IEEE Transactions on Power Electronics*, 2018, vol. 33, no. 5, p. 4488–4497. DOI: 10.1109/TPEL.2017.2723358

[10] HASANIEN, H. M. An adaptive control strategy for low voltage ride through capability enhancement of grid-connected photovoltaic power plants. *IEEE Transactions on Power Systems*, 2016, vol. 31, no. 4, p. 3230–3237. DOI: 10.1109/TPWRS.2015.2466618

[11] DING, G., GAO, F., TIAN, H., et al. Adaptive dc-link voltage control of two-stage photovoltaic inverter during low voltage ride-through operation. *IEEE Transactions on Power Electronics*, 2016, vol. 31, no. 6, p. 4182–4194. DOI: 10.1109/TPEL.2015.2469603

[12] WEN, G., CHEN, Y., ZHONG, Z., et al. Dynamic voltage and current assignment strategies of nine-switch-converter-based DFIG wind power system for low-voltage ride through (LVRT) under symmetrical grid voltage dip. *IEEE Transactions on Industry Applications*, 2016, vol. 52, no. 4, p. 3422–3434. DOI: 10.1109/TIA.2016.2535274

[13] ABBEY, C., JOOS, G. Effect of low voltage ride through (LVRT) characteristic on voltage stability. In *IEEE Power Engineering Society General Meeting 2005*. San Francisco (CA, USA), 2005, vol. 2, p. 1901–1907. DOI: 10.1109/PES.2005.1489659

[14] HU, S., LIN, X., KANG, Y., et al. An improved low-voltage ride-through control strategy of doubly fed induction generator during grid faults. *IEEE Transactions on Power Electronics*, 2011, vol. 26, no. 12, p. 3653–3665. DOI: 10.1109/TPEL.2011.2161776

[15] GOKSU, O., TEODORESCU, R., BAK, C. L., et al. Instability of wind turbine converters during current injection to low voltage grid faults and PLL frequency based stability solution. *IEEE Transactions on Power Systems*, 2014, vol. 29, no. 4, p. 1683 to 1691. DOI: 10.1109/TPWRS.2013.2295261

[16] MOLINAS, M., SUUL, J. A., UNDELAND, T. Low voltage ride through of wind farms with cage generators: STATCOM versus SVC. *IEEE Transactions on Power Electronics*, 2008, vol. 23, no. 3, p. 1104–1117. DOI: 10.1109/TPEL.2008.921169

[17] YANG, Y., BLAABJERG, F. Low-voltage ride-through capability of a single-stage single-phase photovoltaic system connected to the low-voltage grid. *International Journal of Photoenergy*, 2013, no. 1, p. 1–9. DOI: 10.1155/2013/257487

[18] CONROY, J. F., WATSON, R. Low-voltage ride-through of a full converter wind turbine with permanent magnet generator. *IET Renewable Power Generation*, 2007, vol. 1, no. 2, p. 182–189. DOI: 10.1049/iet-rpg:20070033

[19] ANURAG, A., YANG, Y., BLAABJERG, F. Thermal performance and reliability analysis of single-phase PV inverters with reactive power injection outside feed-in operating hours. *IEEE Journal of Emerging and Selected Topics in Power Electronics*, 2015, vol. 3, no. 4, p. 870–880. DOI: 10.1109/JESTPE.2015.2428432

[20] SUBUDHI, B., PRADHAN, R. A comparative study on maximum power point tracking techniques for photovoltaic power systems. *IEEE Transactions on Sustainable Energy*, 2013, vol. 4, no. 1, p. 89–98. DOI: 10.1109/TSTE.2012.2202294

[21] SANGWONGWANICH, A., YANG, Y., BLAABJERG, F. High-performance constant power generation in grid-connected PV systems. *IEEE Transactions on Power Electronics*, 2016, vol. 31, no. 3, p. 1822–1825. DOI: 10.1109/TPEL.2015.2465151

[22] FARAJI, R., REZA NAJI, H., ROUHOLAMINI, A., et al. FPGA-based real time incremental conductance maximum power point tracking controller for photovoltaic systems. *IET Power Electronics*, 2014, vol. 7, no. 5, p. 1294–1304. DOI: 10.1049/iet-pel.2013.0603

[23] MCGRATH, B. P., HOLMES, D. G., GALLOWAY, J. J. H. Power converter line synchronization using a discrete Fourier transform (DFT) based on a variable sample rate. *IEEE Transactions on Power Electronics*, 2005, vol. 20, no. 4, p. 877 to 884. DOI: 10.1109/TPEL.2005.850944

[24] HAN, Y., LUO, M., ZHAO, X., et al. Comparative performance evaluation of orthogonal-signal-generators-based single-phase PLL algorithms - a survey. *IEEE Transactions on Power Electronics*, 2016, vol. 31, no. 5, p. 3932–3944. DOI: 10.1109/TPEL.2015.2466631

[25] SANTOS FILHO, R. M., SEIXAS, P. F., CORTIZO, P. C., et al. Comparison of three single-phase PLL algorithms for UPS applications. *IEEE Transactions on Industrial Electronics*, 2008, vol. 55, no. 8, p. 2923–2932. DOI: 10.1109/TIE.2008.924205

[26] GOLESTAN, S., MONFARED, M., FREIJEDO, F. D., et al. Dynamics assessment of advanced single-phase PLL structures. *IEEE Transactions on Industrial Electronics*, 2013, vol. 60, no. 6, p. 2167–2177. DOI: 10.1109/TIE.2012.2193863

[27] KARIMI-GHARTERMANI, M. Linear and pseudolinear enhanced phased-locked loop (EPLL) structures. *IEEE Transactions on Industrial Electronics*, 2014, vol. 61, no. 3, p. 1464–1474. DOI: 10.1109/TIE.2013.2261035

[28] CIOBOTARU, M., TEODORESCU, R., BLAABJERG, F. A new single-phase PLL structure based on second order generalized integrator. In *Proceedings of the 37th IEEE Power Electronics Specialists Conference*. Jeju (South Korea), 2006, p. 1–6. DOI: 10.1109/pesc.2006.1711988

[29] ZHENG, L., GENG, H., YANG, G. Fast and robust phase estimation algorithm for heavily distorted grid conditions. *IEEE Transactions on Industrial Electronics*, 2016, vol. 63, no. 11, p. 6845–6855. DOI: 10.1109/TIE.2016.2585078

[30] GENG, H., XU, D., WU, B. A novel hardware-based all-digital phase-locked loop applied to grid-connected power converters. *IEEE Transactions on Industrial Electronics*, 2011, vol. 58, no. 5, p. 1737–1745. DOI: 10.1109/TIE.2010.2053338

[31] HUKA, G. B. Y., LI, W., CHAO, P., et al. A comprehensive LVRT strategy of two-stage photovoltaic systems under balanced and unbalanced faults. *International Journal of Electrical Power and Energy Systems*, 2018, vol. 103, p. 288–301. DOI: 10.1016/j.ijepes.2018.06.014

[32] NASIRI, M., ARZANI, A., GUERRERO, J. M. LVRT operation enhancement of single-stage photovoltaic power plants: An analytical approach. *IEEE Transactions on Smart Grid*, 2021, vol. 12, no. 6, p. 5020–5029. DOI: 10.1109/TSG.2021.3108391

[33] JOSHI, J., SWAMI, A. K., JATELY, V., et al. A comprehensive review of control strategies to overcome challenges during LVRT in PV systems. *IEEE Access*, 2021, vol. 9, p. 121804–121834. DOI: 10.1109/ACCESS.2021.3109050

About the Authors …

Zhichao ZHANG was born in 2000 in Taixing city, Jiangsu Province, China. He received his master's degree in Electrical Power Systems from the University of Birmingham in December 2023. Since July 2024, he has been a doctoral student with the School of Electrical Engineering, China University of Mining and Technology. His research interests include new energy power generation technology and power electronics technology.

Qihang LIU was born in 1999 in Lianyungang city, Jiangsu Province, China. He received his master's degree in Electrical Power Systems from the University of Birmingham in December 2023. Since July 2024, he has been conducting integrated technology research at NARI Group Corporation. His research interests include demand-side management, microgrids, and virtual power plants.

Yupei WANG was born in 2000 in Taizhou city, Jiangsu Province, China. He received his Bachelor's degree in Electrical Engineering and Automation from the Harbin University of Science and Technology in June 2022. Since September 2022, he is studying for a master's degree at the School of Electrical Engineering, China University of Mining and Technology. His research interests include relay protection technology in power systems.